Synthesis and supramolecular arrangement of new stearoyl acid-based phenalenone derivatives

Jérémy Godard, David Chapron, Frédérique Bregier, Véronique Rosilio, Vincent Sol

Synthesis and supramolecular arrangement of new stearoyl acid-based phenalenone derivatives

Jérémy Godard,[a] *David Chapron,*[b,c] *Frédérique Bregier,*[a,c] *Véronique Rosilio,*[b,c] *and Vincent Sol* [a,c]*

a Université de Limoges, Laboratoire PEIRENE, EA 7500, 87060 Limoges Cedex, France.

b Université Paris-Saclay, CNRS, Institut Galien Paris-Saclay, 92296 Châtenay-Malabry Cedex, France.

c CNRS, GDR 2025 HappyBio

KEYWORDS. Phenalenone-stearoyl acid conjugate, micelles, vesicles, supramolecular chemistry, self-assembly, CryoTem imaging.

ABSTRACT. Lipid-based photoantimicrobial supramolecular assemblies are promising structures for the development of new photodynamic treatments of wound bacterial infections. Phenalenone (1*H*-phenalene-1-one, PN) has been used to obtain four stearoyl acid-based phenalenone derivatives (PNC_{18}), with different types of linkage and different number of acyl chains. After studying the interfacial properties of these compounds, nano-objects were formed with either pure PNC_{18} or mixtures of PNC_{18} with 1-stearoyl-2-oleoyl-sn-glycero-3-phosphocholine. Morphologies of these nano-objects were analyzed by CryoTEM imaging. The distearoyl glycerol PN derivative appears promising for building photosensitive micelles or vesicles.

1. INTRODUCTION

Wound infections pose serious concerns for public health, being major causes of morbidity and mortality.[1] In addition, they represent a substantial cost burden to healthcare systems. Antibacterial photodynamic therapy (aPDT) appears as an alternative to antibiotics, more particularly against multidrug resistant bacteria.[2] Photodynamic therapy uses photosensitizers (PS) that are activated by absorption of visible light of an appropriate wavelength. According to two different types of mechanisms (type I or type II), photoactivation of photosensitizers leads to the formation of oxygen radicals by electron transfer or of singlet oxygen by energy transfer.[3]

These reactive oxygen species (ROS) are known to be particularly cytotoxic. Various PS have already been studied and have given promising results.[4,5] However, many PS are hydrophobic and, for this reason, they spontaneously aggregate under physiological conditions which leads to a drastic decrease in their effectiveness.[6] To overcome this problem, formulations of PS in micelles and liposomes have been proposed as more efficient delivery systems.[7–9] These formulations allow to solubilize highly hydrophobic compounds in biological media, providing a high local concentration of PS and hence a strong ROS photogeneration. Several synthetic or natural photosensitizers have been successfully tested in this way, for example phenothiazinium dyes,[10,11] indocyanine,[12,13] or tetrapyrrolic compounds.[14,15]

1*H*-phenalen-1-one (PN) is known as a very efficient photosensitizer, due to its high singlet oxygen quantum yield. Otherwise, PN is easy to synthesize and to derivatize.[16] Maisch and co-workers have synthesized quaternary ammonium derivatives of phenalenone, some of them containing long aliphatic hydrocarbon moieties; these latter compounds proved to be effective in bacterial inactivation.[17–19]According to another report, free phenalenone was encapsulated in large unilamellar vesicles made of 1,2-di-oleoyl-sn-glycero-3-phosphocholine. These constructs were used to mimic a photodynamic effect on tryptophan derivatives at a cell membrane/water interface.[20] This study proved that PN retained a sensible photosensitizing power even in a microheterogeneous medium; however this method is barely applicable in vivo, due to the possible release of free PN and hence its unwanted dilution in the medium.

Inclusion of photosensitizers into vesicles can be obtained in two ways. Either the photosensitizer is free and is maintained in the nanostructure by non-covalent interactions with lipid molecules,[21] or the photosensitizer is covalently bound to a lipidic skeleton.[10] Following the works of Temizel *et al*.[22] and Nathan *et al*.,[23] we chose to conjugate

phenalenone with lipophilic alkyl chains. In connection with our research program on the elaboration of new photosensitizers and on drug delivery strategy for PDT applications,[24–26] we designed different neutral phenalenone derivatives carrying one or two stearic chains. These derivatives were further used, either alone or mixed with 1-stearoyl-2-oleoyl-sn-glycero-3-phosphocholine (SOPC) to build supramolecular assemblies ("*phenalenosomes*") or mixed liposomes, respectively.

2. MATERIALS AND METHODS

2.1. Materials

Compounds **1**, **2**, **3** and **4** were synthesized according to a procedure described in our previous paper.[16] Solketal was obtained by reaction between glycerol and acetone according to the ketalization protocol elsewhere described.[27] All other reagents and solvents were purchased from Alfa Aesar, TCI, Carlo Erba, Fisher Chemical, VWR or Sigma Aldrich and were used as received. Column chromatographies were realized with a silica gel 60 (0.015-0.040 mm), and preparative thin layer chromatography with silica gel 60 PF_{254}, both purchased from Merck. NMR analyses were conducted on a Bruker DPX 500 NMR spectrometer, operating at 500 MHz and with tetramethylsilane as reference. High-resolution electrospray ionization mass spectra (HR ESI-MS) were performed by the ICOA/CBM (FR2708) at the University of Orléans (France) with a Bruker Q-TOF maXis mass spectrometer coupled to an Ultimate 3000 RSLC chain (Dionex). The melting points were measured on a Leica VMHB Kofler system without correction.

2.2. Chemical synthesis

*N-((1-((1-oxo-1*H*-phenalen-2-yl) methyl)-1*H*-1,2,3-triazol-4-yl)methyl)stearamide (***1a***).* 363 mg (1 mmol) of **1** and 520 µL (3 mmol) of DIPEA are dissolved in 10 mL of anhydrous DMF. 273 mg (0.9 mmol) of stearoyl chloride are added and the solution is stirred 2 h under inert atmosphere. The solution is then poured into 150 mL of water, the yellow precipitate is filtered, and the solid is dissolved in $CHCl_3$ and dried over $MgSO_4$. The solvent is evaporated, and the crude is purified by column chromatography ($CHCl_3$/MeOH 95:5) to give 133 mg (0.23 mmol, 26%) of a bright yellow powder. **^{1}H-NMR (500 MHz, $CDCl_3$)**: **δ (ppm) =** 8.68 (dd, *J* = 0.7, 7.5 Hz, 1H), 8.24 (d, *J* = 8.0 Hz, 1H), 8.06 (d, *J* = 8.3 Hz, 1H), 7.81 (t, *J* = 7.7 Hz, 1H), 7.79 (d, *J* = 6.2 Hz, 1H), 7.77 (s, 1H), 7.72 (s, 1H), 7.61 (dd, *J* = 8.0, 7.4 Hz, 1H), 6.08 (t, *J* = 5.6 Hz, 1H), 5.55 (s, 2H), 4.52 (d, *J* = 5.5 Hz, 2H), 2.17 (t, *J* = 7.6 Hz, 2H), 1.25 (m, 30H), 0.87 (t, *J* = 6.8 Hz, 3H). - **^{13}C-NMR (125 MHz, $CDCl_3$)**: **δ (ppm) =** 183.81, 173.11, 144.75, 141.22, 135.57, 133.40, 132.72, 132.67, 132.07, 131.13, 128.84, 127.41, 127.36, 126.90, 126.81, 123.17, 48.99, 36.63, 35.00, 31.93, 29.70 (3C), 29.68, 29.66 (2C), 29.65, 29.61, 29.47, 29.36, 29.33, 29.30, 25.62, 22.69, 14.11. - **MS:** HRMS (ESI^+), calcd for $C_{35}H_{49}N_4O_2$ $[M+H]^+$: 557.385003, found 557.384404. - **MW**: 556.8 g/mol. **MP:** 148 °C.

*(1-oxo-1*H*-phenalen-2-yl)methyl stearate (***2a***).* 211 mg (1 mmol) of **2** and 191 µL (1.1 mmol) of DIPEA are dissolved in 20 mL of anhydrous DMF under inert atmosphere. 333 mg (1.1 mmol) of stearoyl chloride are added and a yellow precipitate appears rapidly. The reaction is left 24 h under stirring at room temperature, and then poured into 100 mL of water. The solid is filtered off and washed with cold ethanol. The residual impurities are removed by column chromatography (eluent : $CHCl_3$/MeOH 98:2) to yield 133 mg (0.29 mmol, 29%) of a bright yellow powder. **^{1}H-NMR (500 MHz, $CDCl_3$)**: **δ (ppm) =** 8.67 (dd, *J* = 0.95, 6.4 Hz, 1H), 8.22 (d, *J* = 6.0 Hz, 1H), 8.04 (d, *J* = 8.2 Hz, 1H), 7.79 (m, 3H), 7.61 (dd, *J* = 7.3, 0.8 Hz, 1H), 5.21

(d, *J* = 0.6 Hz, 2H), 2.42 (t, *J* = 7.6 Hz, 2H), 1.69 (q^5, *J* = 7.5 Hz, 2H), 1.25 (m, 28H), 0.87 (t, *J* = 6.9 Hz, 3H). - **^{13}C-NMR (125 MHz, $CDCl_3$)**: **δ (ppm) =** 184.04, 173.65, 139.33, 135.03, 134.57, 132.07, 131.93, 131.74, 130.68, 129.15, 127.33, 127.27, 127.24, 126.76, 61.30, 34.39, 31.93, 29.70 (4C), 29.66 (3C), 29.60, 29.49, 29.36, 29.29, 29.20, 25.03, 22.69, 14.12. - **MS:** HRMS (ESI^+), calcd for $C_{32}H_{45}O_3$ $[M+H]^+$: 477.336322, found 477.336134. - **MW**: 476.70 g/mol. - **MP:** 92 °C.

*N-((1-oxo-1*H*-phenalen-2-yl)methyl)stearamide (***3a***).* 1.2 g (4.88 mmol) of **3** is dissolved in 200 mL of anhydrous DMF with 1.78 mL (12.42 mmol) of DIPEA and stirred 20 min under inert atmosphere. 1.63 g (5.37 mmol) of stearoyl chloride is added cautiously. A yellow precipitate appears rapidly. The reaction is left 24 h under inert atmosphere and is then poured in 1.5 L of cold water. The yellow precipitate is filtered and washed with cold ethanol. The remaining impurities are eliminated by column chromatography (eluent: CH_2Cl_2/MeOH 9:1) and the product is crystallized in petroleum ether to yield 1.31 g (2.75 mmol, 56%) of a bright yellow powder. **^{1}H-NMR (500 MHz, $CDCl_3$)**: **δ (ppm) =** 8.65 (dd, *J* = 1.0, 6.4 Hz, 1H), 8.22 (d, *J* = 8.0 Hz, 1H), 8.02 (d, *J* = 8.2 Hz, 1H), 7.83 (s, 1H), 7.80 (d, *J* = 7.7 Hz, 1H), 7.79 (d, *J* = 7.7 Hz, 1H), 7.60 (dd, *J* = 7.2, 0.9 Hz, 1H), 6.41 (t, *J* = 5.7 Hz, 1H), 4.42 (d, *J* = 6.3 Hz, 2H), 2.17 (t, *J* = 7.6 Hz, 2H), 1.62 (q^5, *J* = 7.5 Hz, 2H), 1.25 (m, 28H), 0.88 (t, *J* = 7.0 Hz, 3H). - **^{13}C-NMR (125 MHz, $CDCl_3$)**: **δ (ppm) =** 185.73, 173.20, 140.08, 136.05, 135.26, 132.05 (2H), 131.84, 130.59, 129.20, 127.50, 127.23, 127.12, 126.89, 39.77, 36.89, 31.93, 29.70 (3H), 29.66, 29.65, 29.63, 29.57, 29.48, 29.36, 29.34, 29.29, 25.70, 22.70, 14.11. - **MS:** HRMS (ESI^+), calcd for $C_{32}H_{46}NO_2$ $[M+H]^+$: 476.352306, found 476.351983. - **MW**: 475.72 g/mol. - **MP:** 118 °C.

*2-(((2,2-dimethyl-1,3-dioxolan-4-yl)methoxy)methyl)-1*H*-phenalen-1-one (***5***).* 456 mg (2 mmol) of **4**, 1.98 g (8 mmol) of solketal and 100 mg of tetrabutylammonium iodide (TBAI) are

dissolved in 20 mL of CH_2Cl_2 and 20 mL of 5 M NaOH. The biphasic mixture is vigorously stirred during 5 h at room temperature. After adding of 20 mL of CH_2Cl_2 and 20 mL of water, the organic phase is collected, dried over $MgSO_4$ and evaporated. The crude is purified by column chromatography ($CHCl_3$) to obtain a viscous oil that solidified at room temperature under strong trituration with 77% yield (501 mg, 1.54 mmol). **^{1}H-NMR (500 MHz, $CDCl_3$)**: **δ (ppm) =** 8.65 (dd, *J* = 1.1, 7.4 Hz, 1H), 8.22 (dd, *J* = 0.7, 8.1 Hz, 1H), 8.02 (d, *J* = 8.3 Hz, 1H), 7.87 (s, 1H), 7.80 (m, 2H), 7.62 (dd, *J* = 7.2, 8.2 Hz, 1H), 4.70 (d, *J* = 1.3, 15.0 Hz, 1H), 4.66 (d, *J* = 1.3, 15.0 Hz, 1H), 4.44 (q^5d, *J* = 0.6, 5.9 Hz, 1H), 4.15 (dd, *J* = 6.5, 8.2 Hz, 1H), 3.84 (dd, *J* = 6.5, 8.2 Hz, 1H), 3.77 (dd, *J* = 5.8, 10.0 Hz, 1H), 3.70 (dd, *J* = 5.1, 10.0 Hz, 1H), 1.47 (s, 3H), 1.40 (s, 3H). - **^{13}C-NMR (125 MHz, $CDCl_3$)**: **δ (ppm) =** 184.45, 137.64, 136.49, 134.97, 132.05, 131.48, 131.42, 129.20, 127.68, 127.10, 127.05, 126.80, 109.57, 74.84, 72.30, 68.25, 66.79, 26.84, 25.48. - **MS:** HRMS (ESI^+), calcd for $C_{20}H_{21}O_4$ $[M+H]^+$: 325.143436, found 325.143247. - **MW**: 324.38 g/mol. - **MP:** 78 °C.

*2-((2,3-dihydroxypropoxy)methyl)-1*H*-phenalen-1-one (***6***).* 800 mg (2.47 mmol) of **5** is dissolved in 10 mL of MeOH and 4 mL of 37% HCl are cautiously added. The solution is stirred 20 min at ambient temperature and is then poured into 300 mL of water. The product is extracted with CH_2Cl_2, the solvent is evaporated, and the crude is purified by column chromatography ($CHCl_3$/MeOH 95:5 then 98:2) to give 671 mg (2.36 mmol, 97%) of a yellow powder. **^{1}H-NMR (500 MHz, $CDCl_3$)**: **δ (ppm) =** 8.67 (dd, *J* = 1.0, 7.4 Hz, 1H), 8.23 (dd, *J* = 0.6, 8.0 Hz, 1H), 8.04 (d, *J* = 8.1 Hz, 1H), 7.80 (m, 3H), 7.63 (dd, *J* = 7.2, 8.1 Hz, 1H), 4.66 (dd, *J* = 1.0, 13.2 Hz, 1H), 4.63 (dd, *J* = 1.0, 13.2 Hz, 1H), 4.04 (q^5, *J* = 5.0 Hz, 1H), 3.78 (m, 4H), 3.26 (s, 1H), 2.33 (s, 1H). - **^{13}C-NMR (125 MHz, $CDCl_3$)**: **δ (ppm) =** 184.74, 138.97, 136.02, 135.17, 132.02, 131.89, 131.78, 130.78, 129.18, 127.39, 127.21, 127.16, 126.81, 72.71, 70.69, 68.94, 64.02. -

MS: HRMS (ESI^+), calcd for $C_{17}H_{17}O_4$ $[M+H]^+$: 285.112390, found 285.112135. - **MW**: 284.31 g/mol. - **MP:** ND.

*2-hydroxy-3-((1-oxo-1*H*-phenalen-2-yl)methoxy)propyl stearate (***6a***).* 668 mg (2.3 mmol) of **6** and 1.5 mL (10.8 mmol) of Et_3N are dissolved in 57 mL of DMF and placed under inert atmosphere. 1.38 g (4.6 mmol) of stearoyl chloride is slowly added. A yellow precipitate appears, and the mixture is stirred 100 min under inert atmosphere. The suspension is then poured into 1 L of water, and the precipitate is filtered, dissolved in $CHCl_3$, dried over $MgSO_4$ and evaporated. The crude is purified by column chromatography ($CHCl_3$/MeOH 98:2) to give 515 mg (0.94 mmol, 41%) of a yellow-orange powder identified as the product **6a** and 36 mg (0.044 mmol, 1.9 %) identified as **6b**. **^{1}H-NMR (500 MHz, $CDCl_3$)**: **δ (ppm) =** 8.67 (dd, *J* = 1.0, 7.4 Hz, 1H), 8.23 (dd, *J* = 0.6, 8.0 Hz, 1H), 8.04 (d, *J* = 8.1 Hz, 1H), 7.81 (m, 3H), 7.63 (dd, *J* = 7.1, 8.1 Hz, 1H), 4.68 (dd, *J* = 1.0, 13.6 Hz, 1H), 4.64 (dd, *J* = 1.0, 13.6 Hz, 1H), 4.27 (dd, *J* = 4.7, 11.4 Hz, 1H), 4.23 (dd, *J* = 5.9, 11.4 Hz, 1H), 4.17 (q^5, *J* = 5.2 Hz, 1H), 3.77 (dd, *J* = 4.0, 10.0 Hz, 1H), 3.71 (dd, *J* = 6.3, 10.0 Hz, 1H), 2.36 (t, *J* = 7.5 Hz, 2H), 1.65 (m, 4H), 1.25 (m, 26H), 0.89 (t, *J* = 7.0 Hz, 3H). - **^{13}C-NMR (125 MHz, $CDCl_3$)**: **δ (ppm) =** 184.58, 173.99, 138.47, 136.13, 135.11, 132.05, 131.78, 131.69, 130.69, 129.69, 129.19, 127.47, 127.19, 127.14, 126.81, 72.04, 68.98, 68.70, 65.32, 34.21, 31.93, 29.70 (4C), 29.66 (2C), 29.61, 29.55, 29.47, 29.36, 29.26, 29.15, 24.95, 22.69, 14.12. - **MS:** HRMS (ESI^+), calcd for $C_{35}H_{51}O_5$ $[M+H]^+$: 551.373101, found 551.372487. - **MW**: 550.78 g/mol. - **MP:** 45 °C.

*3-((1-oxo-1*H*-phenalen-2-yl)methoxy)propane-1,2-diyl distearate (***6b***).* 97 mg (0.37 mmol) of triphenylphosphine is dissolved in 1.5 mL of anhydrous THF and placed at -10 °C under inert atmosphere. 84 µL (0.43 mmol) of diisopropyl azodicarboxylate (DIAD) are slowly added. A white precipitate appears. 105 mg (0.35 mmol) of stearoyl chloride and 187 mg (0.34 mmol) of

6a dissolved in 2 mL of anhydrous THF are added dropwise. The cold bath is removed, and the reaction is left 2 h under stirring at room temperature. The solvent is then evaporated, and the crude is purified by column chromatography ($CHCl_3$) to yield 139 mg (0.17 mmol, 50%) of **6b** as a bright yellow powder after evaporation in diethyl ether at 15 °C under vacuum. **^{1}H-NMR (500 MHz, $CDCl_3$)**: **δ (ppm) =** 8.65 (dd, *J* = 0.9, 7.3 Hz, 1H), 8.22 (d, *J* = 7.8 Hz, 1H), 8.03 (d, *J* = 8.3 Hz, 1H), 7.81 (m, 3H), 7.63 (dd, *J* = 7.4, 8.1 Hz, 1H), 5.37 (q^5, *J* = 5.0 Hz, 1H), 4.66 (dd, *J* = 1.1, 14.9 Hz, 1H), 4.63 (dd, *J* = 1.1, 14.9 Hz, 1H), 4.43 (dd, *J* = 3.9, 11.9 Hz, 1H), 4.28 (dd, *J* = 6.2, 11.9 Hz, 1H), 3.80 (d, *J* = 5.3 Hz, 2H), 2.36 (t, *J* = 7.5 Hz, 2H), 2.33 (t, *J* = 7.5 Hz, 2H), 1.66 (q5, *J* = 7.3 Hz, 4H), 1.58 (m, 4H), 1.25 (m, 52H), 0.89 (t, *J* = 6.9 Hz, 6H). - **^{13}C-NMR (125 MHz, $CDCl_3$)**: **δ (ppm) =** 184.32, 173.48, 173.15, 137.46, 136.39, 135.00, 132.06, 131.52 (2C), 130.43, 129.16, 127.64, 127.11, 127.04, 126.81, 70.15, 69.60, 68.22, 62.66, 34.41 (2C), 34.17 (2C), 31.94 (2C), 29.71 (4C), 29.67 (2C), 29.64 (2C), 29.50 (2C), 29.37 (2C), 29.32 (2C), 29.29 (2C), 29.15 (2C), 29.13 (2C), 25.02 (2C), 24.93 (2C), 22.70 (2C), 14.12 (2C). - **MS:** HRMS (ESI^+), calcd for $C_{53}H_{85}O_6$ $[M+H]^+$: 817.634067, found 817.634138. - **MW**: 817.25 g/mol. - **MP:** 63 °C.

2.3. Surface pressure measurements.

Surface pressure-surface area (π-A) measurements of monolayers of 1-stearoyl-2-oleoyl-sn-glycero-3-phosphocholine (SOPC, Avanti Polar Lipids, Inc., Alabaster, AL, USA) and phenalenone derivatives were performed using a thermostated Langmuir film trough (775.75 cm^2, Biolin Scientific, Finland) enclosed in a plexiglas box and protected from light. All experiments were performed at 22 ±1 °C. Prior to monolayer deposition, compression-expansion cycles were performed on ultrapure water subphase (Millipore Milli-Q Direct 8 water purification system) to verify that the surface pressure did not exceed 0.1 mN/m. SOPC and the

phenalenone derivatives solubilized in chloroform/methanol (9:1 v/v; both solvents > 99.80% pure, Carlo Erba reagents) were spread at air/water interface, and the system was left for 15 min to allow complete evaporation of the organic solvents. Monolayer compression was performed at a speed of 6 $Å^2$.$molecule^{-1}$.min^{-1}. Results are mean values of at least 3 measurements. The surface compressional moduli (C_s^{-1}) of monolayers were calculated from the equation (1):

$$C_S^{-1} = -A\frac{d\pi}{dA} \quad (1)$$

where A is the molecular area, and dπ the surface pressure change.

2.4. Formation of nano-assemblies.

Pure **6b** or SOPC and phenalenone derivatives were dissolved in a mixture of chloroform and methanol (9:1, v/v) and the solvents were evaporated at 40 °C under reduced pressure. The resulting film was hydrated with pure water at room temperature to obtain a concentration of 2 mg lipids/mL, and the resulting lipid suspension was then sonicated for 10 min by a series of 10 s-on/10 s-off cycles (i.e., 20 min in total) using a Vibracell 75041 probe sonicator (750 W, 20 kHz, Bioblock Scientific, Aalst, Belgium) at 20% amplitude. The suspension of pure **6b** was used with no further treatment, while the other formulations were centrifuged at 2,000g for 25 min. All of the obtained nano-assembly suspensions were stored in darkness at 4 °C.

2.5. Analysis of the nano-assemblies by cryogenic transmission electron microscopy (CryoTEM).

The morphology of the nano-assemblies was analyzed by cryogenic transmission electron microscopy using a JEOL 2200FS TEM (JEOL USA, Inc., Peabody, MA, U.S.A.) equipped with a Gatan Ultrascan 2K camera (Gatan, Evry, France). An aliquot (5 µL) of each suspension was

deposited onto a perforated carbon-coated copper grid (TedPella, Inc.). After removal of excess liquid with a filter paper, the grid was quickly frozen in liquid ethane at -180 °C and mounted on the cryo-holder for microscopic analysis.

3. RESULTS AND DISCUSSION

3.1. Synthesis of the PN derivatives.

The new PN derivatives were synthesized based on previously described functionalizations of PN.[16] Hydroxyl and amino moieties were the starting groups for the formation of ester or amide linkages with stearic acid as a model fatty acid.

The first three PN-stearic acid derivatives were obtained by reaction of stearoyl chloride with phenalenone amino derivatives **1** and **3** and phenalenone hydroxy derivative **2** (**Scheme 1**).After purification, products **1a**, **2a** and **3a,** comprising one stearoyl chain were obtained in 26% to 59% yields.

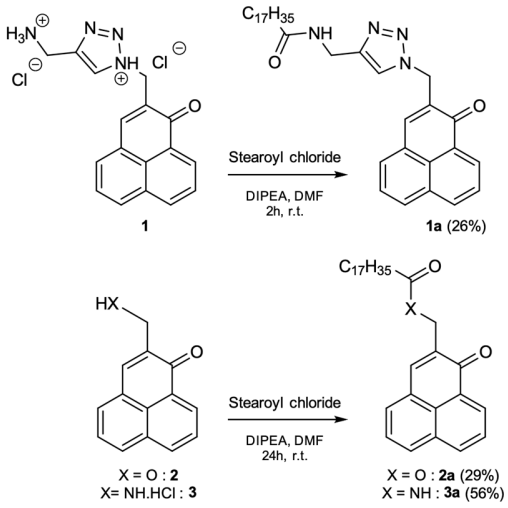

Scheme 1. Synthesis of phenalenone derivatives **1a**, **2a** and **3a** by action of stearoyl chloride on amino- and hydroxy- phenalenones.

The glycerol pattern was chosen to mimic natural lipids, e.g. glycerophospholipids (**Scheme 2**). The glycerol moiety was added by reacting racemic solketal with **4** in a well-known phase transfer catalysis.[16] Compound **5**, obtained in good yield, was deprotected by acid hydrolysis to give **6** in a quasi-quantitative yield. The two alcohol moieties were expected to react with stearoyl chloride but, compound **6a**, only substituted on the primary alcohol, was the main product of the reaction. Very small amounts of the doubly substituted compound **6b** were actually isolated.

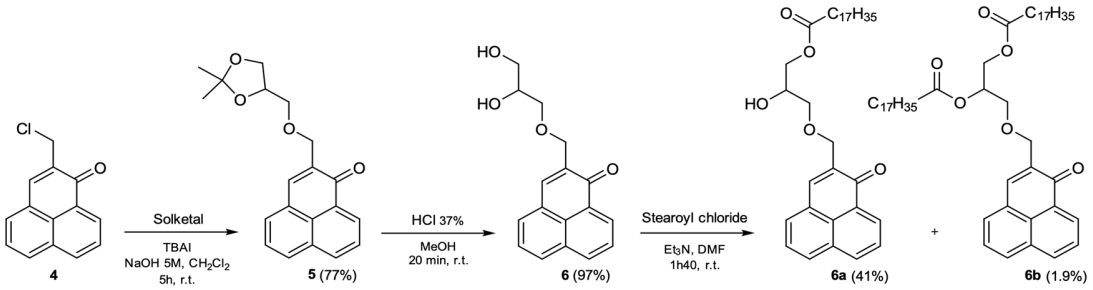

Scheme 2. Synthetic route of mono and doubly substituted PN **6a** and **6b**.

The secondary alcoholic function of compound **6** showed a poor reactivity; the Mitsunobu reaction seemed therefore to be a good alternative to overcome this problem (**Scheme 3**). The presence of several by-products made the purification somewhat tricky, but **6b** was obtained in good yield (50%).

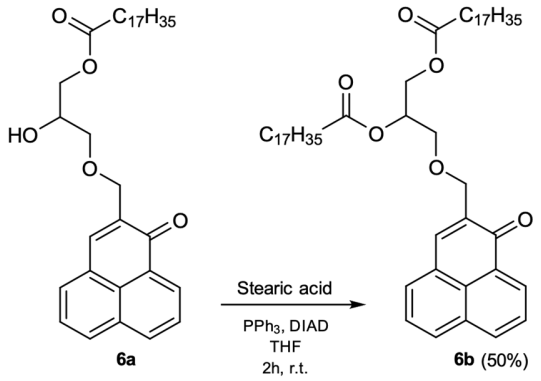

Scheme 3. Synthesis of the doubly substituted phenalenone **6b** by the Mitsunobu reaction

All the compounds were characterized by ^{1}H, ^{13}C NMR and HRMS and all the recorded spectra showed the expected signals (See Supporting Information).

3.2 Two-dimensional and supramolecular arrangements of phenalenone derivatives

The interfacial properties of **1a**, **2a**, **3a** and **6b** were analyzed by surface pressure measurements. Mean isotherms of monolayers of the four compounds are presented in **Fig. 1**. Their characteristic values are summarized in **Table 1**. Compounds **1a**, **2a** and **3a** can be compared to stearic acid, from which they are derived. However, none of them did show the typical characteristics of stearic acid, namely: onset molecular area at 27 $Å^2$, liquid expanded-liquid condensed state transition at 30 mN/m, high collapse surface pressure (50-55 mN/m) and small limiting molecular area (1820 $Å^2$).[28–30] The presence of the linker and of the phenalenone moiety leads to an increase of the molecular area and to a lowering of both the surface pressure at collapse and the surface pressure at which the liquid expanded-liquid condensed state transition occurs. The three compounds may be classified as follows, according to the molecular area enlargement induced by their linker: ester (**2a**) > amide (**3a**) > amide

triazole (**1a**). Compound **1a** exhibits the closest molecular area to that of stearic acid. This can be explained by the greater flexibility provided by the amide-triazole linker in comparison with the ester and amide ones. This greater flexibility may have two consequences: it may (i) lead to progressive immersion of the non-lipid fraction in the subphase while the compression of the monolayer is in progress or (ii) allow the rearrangement of phenalenone molecules at the interface so that they can more strongly interact with each other. The relatively low surface pressure at collapse and low maximal compressibility modulus make the immersion of the phenalenone moieties in the subphase more plausible than a strong phenalenone-phenalenone interaction in the air phase. The significant depth at which phenalenone is immersed reduces its influence on the interface **(Fig. 2**). The flexibility of the linker, however, may also promote phenalenone-phenalenone interactions in the subphase, which would contribute to the reduction of the molecular area of **1a**.

The ester bond in **2a** is responsible for the most significant increase in molecular area between 0 and 15 mN/m, accounting for the presence of phenalenone at the interface. However above 15 mN/m, a strong reduction of the molecular area is observed up to 27 $Å^2$, below which surface pressure increases again. It seems that the monolayer reaches its limit of compression at about 15 mN/m, and that further compression leads to the formation of multilayers (**Fig. 1 and 2**). This assumption is supported by the molecular areas measured above 16 mN/m, which are much smaller than the cross-section of a methylene group.[28]

Compound **3a** exhibits an intermediary limiting molecular area. It also leads to higher surface pressures and compressibility moduli (**Fig. 1, Table 1**). Apparently, the short and hydrophobic amide linker maintains phenalenone groups close to the interface until collapse (**Fig. 2**). It thus affects much more the surface tension as compared with phenalenone in **1a**. It is interesting to

note that the LE-LC transition of all the three phenalenone derivatives occurs around 15 mN/m (dotted lines in **Fig. 1**), which could be the surface pressure at which most phenalenone groups are expelled from the plane of the interface.

All PN-stearic acid derivative monolayers are less organized than those of their precursor,[28,30] as deduced from their relatively low maximal compressibility moduli (stearic acid > 500 mN/m > **3a** > **1a** > **2a**). Compound **3a** forms the most rigid monolayers, probably due to the presence of phenalenone molecules at the interface, even at high surface pressures.

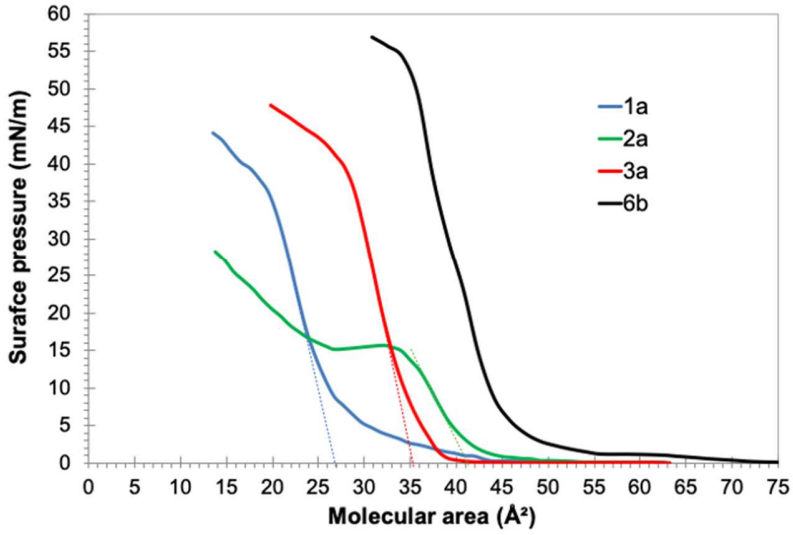

Figure 1. Compression isotherms of pure compounds spread at the air/water interface

Table 1. Characteristics of the compression isotherms of the studied pure phenalenone derivatives

Phenalenone derivative	Surface pressure at collapse (mN/m)	Molecular area at collapse (Å^2)	Maximal compressibility modulus (mN/m)
1a	37.0	19.8	119.4
2a	15.8	27-34.4	88.1
3a	41.2	28.0	185.8
6b	54.0	34.8	249.1

Compound **6b** with its two alkyl chains can be compared to distearoylphosphatidylcholine (DSPC). Like stearic acid, DSPC has been studied by many authors.[31–33] Its interfacial behavior is characterized by a surface pressure higher than 60 mN/m at collapse corresponding to a molecular area of 48 Å^2, as deduced from surface pressure measurements and grazing incidence X-ray diffraction experiments as well.[34] Considering that the presence of phenalenone at the interface should lead to an additional enlargement of the molecular area, a limiting molecular area higher than 60 Å^2 would be expected. However, **6b** exhibits much smaller molecular area and surface pressure than DSPC at collapse **(Table 1**). This accounts for the immersion of the phenalenone groups in the subphase during compression, but also for the strong interactions between these groups.

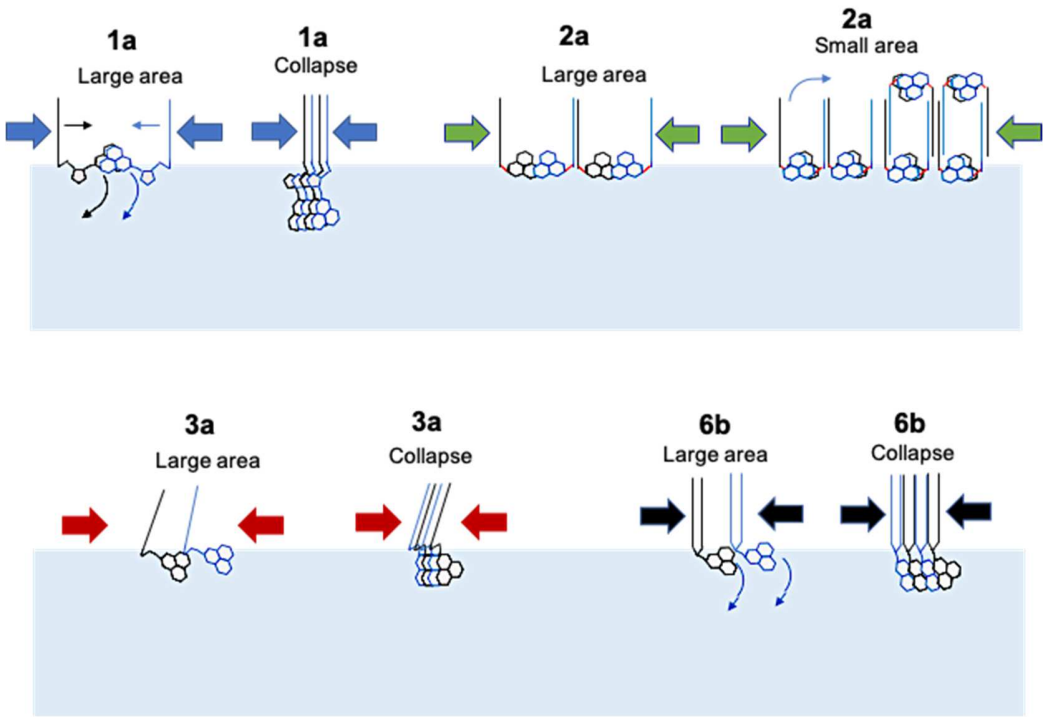

Figure 2. Putative organization of phenalenone derivatives at the air-water interface

Owing to its similarity with glycerophospholipids, **6b** was used to form vesicles, either pure or mixed with 1-stearoyl-2-oleoyl-sn-glycero-3-phosphocholine (SOPC, 75, 50 and 25 mol%). Compounds **1a** and **3a** were mixed with SOPC (90 mol% for **1a** and 60 and 90 mol% for **3a**) in an attempt to obtain vesicles. Compound **2a**, forming disorganized and unstable monolayers, was not studied.

It is possible to build liposome-like porphysomes from pure lipid-porphyrin conjugates.[35,36] The stability of these vesicles specifically depends on the chemical structure of the building block.[37] In the same manner, pure **6b** could self-assemble into *phenalenosomes*. However, the CryoTEM images in **Fig. 3(I, II)** reveal that this compound self-assembles into massive nanoplatelet-like objects (several hundred nm), consisting of stacks of 5.5 to 6.5 nm thick bilayers. These bilayers are thicker than those observed with glycerophospholipid bilayers (4 nm

for SOPC, 5 nm for DSPC).[38–40] This would account for the positioning of the phenalenone moieties in the polar head region rather than between the hydrophobic chains, as also deduced from monolayer studies. Mixed with SOPC, **6b** hampers the formation of stable SOPC multilamellar vesicles (MLV) and seems to promote their transformation into LUV, SUV, and bilayer leaflets (**Fig.3 (III-VI)).** Figure 3 (IV) shows multilamellar vesicles with stacked bilayers, and loose, deformed, bilayers gradually separating from each other. These expanded bilayers evolve into bilayers sheets. It is noteworthy that the concentrations of the phenalenone derivative in the SOPC-**6b** mixtures are very high compared with the usual loading rate of hydrophobic compounds in liposome membranes, which rarely exceeds 5%.[14,41,42] Due to the high concentration of **6b,** phase separation may occur, as suggested by the coexistence of several different objects.

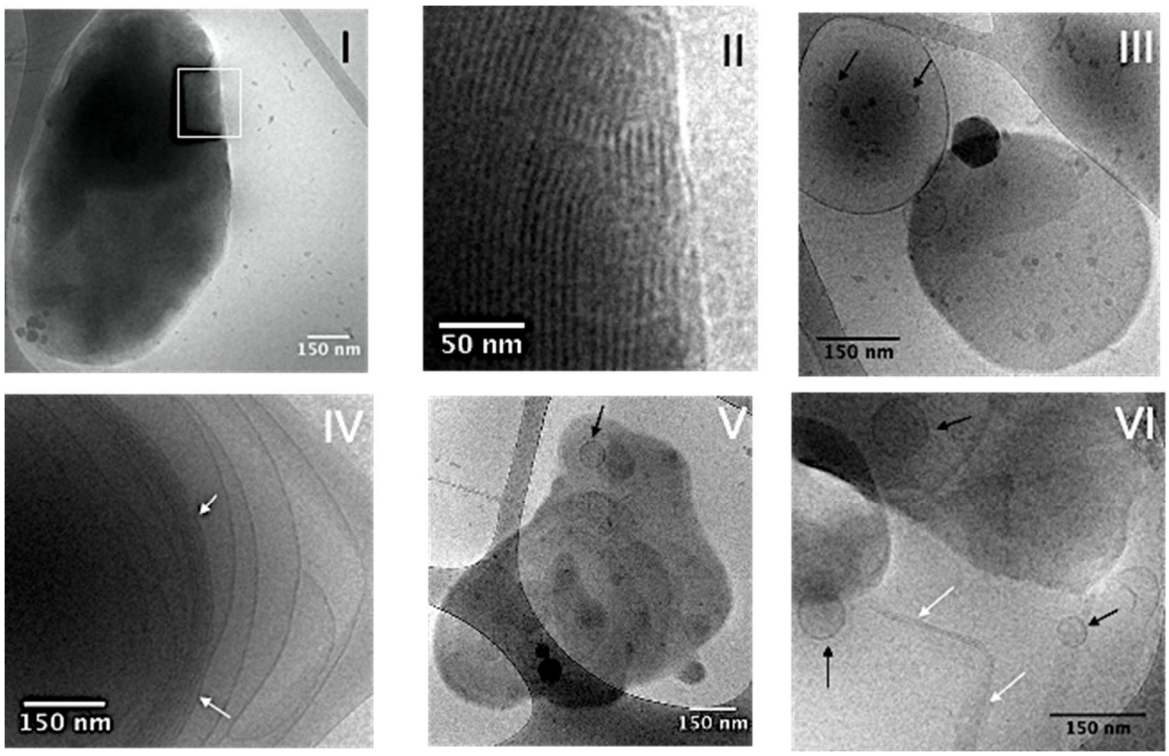

Figure 3. Morphology of objects formed by pure **6b** (I,II) and its mixtures with SOPC (III, IV: 75 mol%, V: 50 mol%, VI: 25 mol% **6b**). (II) is an enlargement of the nanoplatelet (I) showing the stacked bilayers. White arrows indicate the zones where stacked bilayers are visible. Black arrows point to SUV.

The CryoTEM images in **Fig. 4** illustrate the behavior of **1a** and **3a** in the presence of SOPC. At high concentrations, **3a** forms bilayer stacks (not shown) with a morphology similar to that of **6b**, although they appear to be less dense and smaller in size than those of the latter. Twisted ribbons, unilamellar and oligolamellar vesicles, numerous SUV accumulated onto the carbon mesh of the grid, as well as small dense nanoparticles (about 50 nm in diameter) are also observed (**Fig. 4 (I, II)).** Although it is not clear whether these nanoparticles are really obtained by self-association of **3a**, they do not look like contaminants, having a much more spherical appearance than ethane crystals. They are not observed at 10 mol% **3a (Fig. 4 (III)**). With **1a** (10 mol%), a profusion of onion-like multilamellar liposomes is observed (not shown) as expected in SOPC vesicle suspensions. However, there are also a multitude of oligolamellar vesicles along with interwoven bilayer sheets, which seem to result from the destructuration of vesicles (**Fig. 4 (IV)**). Obviously, at low concentration (10 mol%) **1a** and **3a** induce some multilamellar-to-unilamellar transition in vesicles, but also transformation of vesicles into bilayer sheets.

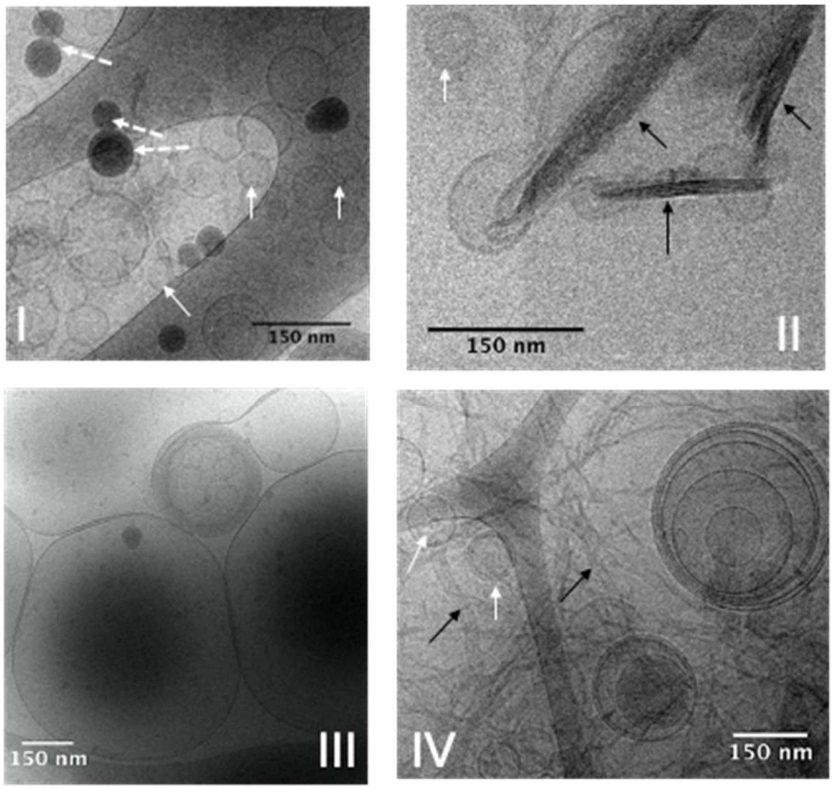

Figure 4. Morphology of objects formed by **3a**/SOPC mixtures (I, II: 40 mol% **3a**; III: 10 mol% **3a**) and **1a**/SOPC (IV: 10 mol% **1a**). Black arrows indicate bilayers and fibers; white plain arrows indicate the SUVs and doted white arrows indicate nanoparticles.

Multilamellar-to-unilamellar transition has been described in the literature in systems containing cationic lipids or surfactants, or in systems containing peptides or peptide-like molecules. In both cases, electrostatic interactions between bilayers lead to the destabilization of multilamellar vesicles and the formation of unilamellar ones,[43,44] but these interactions cannot be invoked in the present work. The formation of stacked bilayers in pure **6b** nano-assemblies could be explained by strong π-π interactions between phenalenone molecules in the plane of the leaflets and between bilayers (**Fig. 5**). Indeed, in systems containing **6b** (pure or mixed with SOPC), there are two contributions to the stacking of molecules: the lateral interaction between

the hydrophobic chains and the lateral interaction between the phenalenone groups. The lateral interaction between phenalenone groups can be applied in the same bilayer (**Fig. 5, II**), or between two adjacent bilayers, as shown in **Fig. 5 (I)**. The CryoTEM images tend to show that the lateral interaction between the phenalenone groups of **6b** is stronger than that between its hydrophobic chains. In the case described in **Fig. 5 (II, III)**, SOPC-**6b** bilayer deformation is expected because the strong phenalenone-phenalenone interaction leads to the formation of rigid domains coexisting with fluid domains of SOPC. In the case depicted in **Fig. 5 (I, III)**, stacked bilayers are formed due to the strong interaction between phenalenone molecules emerging from adjacent bilayers. Thorough physicochemical characterization is in progress to confirm this hypothesis.

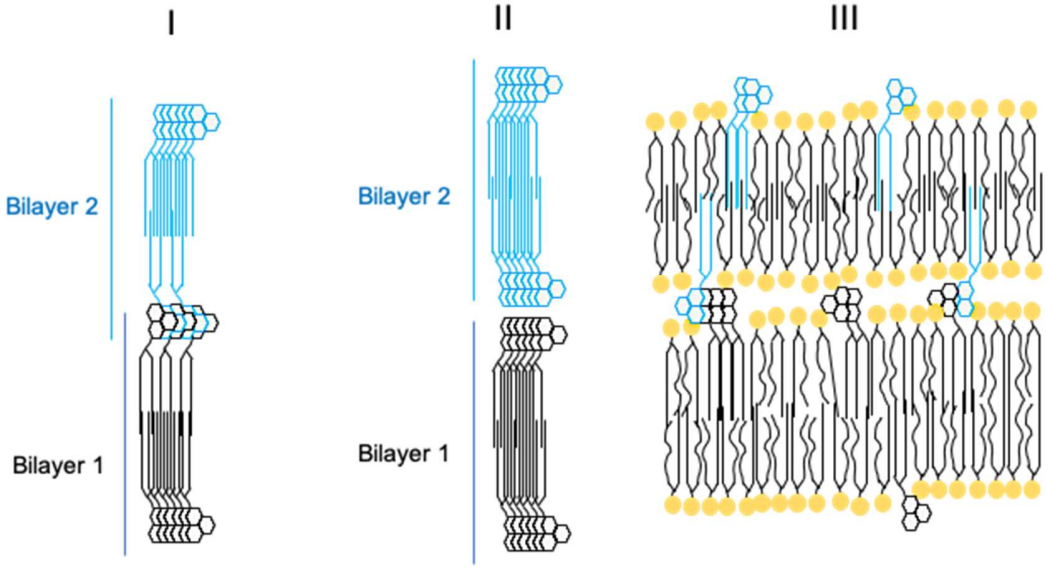

Figure 5: Putative organization of **6b** in pure and mixed bilayers. (I) Lateral and interbilayer stacking of phenalenone molecules, (II) lateral stacking of phenalenone molecules without

interbilayer interaction, (III) domains formation and interbilayer stacking controlled by **6b** in SOPC-**6b** systems.

4. CONCLUSIONS

In this work and for the first time, four new stearic-acid based phenalenone derivatives (PNC_{18}), with variations in the type of linkage and the number of acyl chains, have been synthesized. The destructuring effect of all the studied phenalenone derivatives on phospholipid organization results from the insertion of these molecules into the phospholipid bilayers, affecting the packing of the phospholipid molecules and the curvature of the bilayer, as well as the fragmentation of the vesicles during sonication. Sonication leads to the formation of stable and metastable lipid assemblies, which may undergo further spontaneous transformation (**Fig. 3 (IV)**, and **Fig. 4 (II, III, IV)** depending on the stability of the mixtures of phospholipid and phenalenone derivative. Obviously, phenalenone derivatives, at the studied concentrations, perturb the formation and stability of SOPC vesicles rather than they control the formation of a specific kind of nano-assembly. Lower concentrations of phenalenone derivatives could be tested for micelle formation or successful encapsulation in stable vesicles with photodynamic properties. Only compound **6b** seems to be able of self-assembly into stable bilayer stacks upon sonication. These nanoplatelets are quite large and exhibit various shapes. It would be interesting to evaluate whether the nanostructuring of this PN derivative leads to an improved photoinactivating activity against bacteria as compared with free phenalenone.

DECLARATIONS OF COMPETING INTEREST

The authors report no declarations of interest.

ACKNOWLEDGEMENT

The authors acknowledge “Région Nouvelle-Aquitaine” for financial support. Dr Sylvain Trepout, (Multimodal Imaging Centre, US43/CNRS UMS 2016, Institut Curie, Orsay, France) for assistance in CryoTEM experiments, Dr Cyril Colas (ICOA, Orléans University, France) for the HRMS experiments, Dr Yves Champavier (BISCEm, Limoges University, France) for the NMR experiments and Dr. Michel Guilloton for manuscript editing.

APPENDIX A. SUPPLEMENTARY DATA

The following files are available free of charge.

^{1}H and ^{13}C NMR spectra, and HRMS spectra. (file type, i.e., PDF)

AUTHOR INFORMATION

Corresponding Author

Author to whom correspondence should be addressed: Vincent SOL (vincent.sol@unilim.fr).

ABBREVIATIONS

PN, 1*H*-Phenalen-1-one; PNC_{18}, stearic acid PN derivative; SOPC, 1-stearoyl-2-oleoyl-sn-glycero-3-phosphocholine; DSPC, distearoylphosphatidylcholine.

REFERENCES

[1] J. O’Neill, Tackling drug-resistant infections globally: final report and recommendations, (2016). https://amr-review.org/sites/default/files/160518_Final%20paper_with%20cover.pdf (accessed November 26, 2020).

[2] M. Wainwright, T. Maisch, S. Nonell, K. Plaetzer, A. Almeida, G.P. Tegos, M.R. Hamblin, Photoantimicrobials—are we afraid of the light?, The Lancet Infectious Diseases. 17 (2017) e49–e55. https://doi.org/10.1016/S1473-3099(16)30268-7.

[3] B. Yang, Y. Chen, J. Shi, Reactive Oxygen Species (ROS)-Based Nanomedicine, Chem Rev. 119 (2019) 4881–4985. https://doi.org/10.1021/acs.chemrev.8b00626.
[4] J. Ghorbani, D. Rahban, S. Aghamiri, A. Teymouri, A. Bahador, Photosensitizers in antibacterial photodynamic therapy: an overview, LASER THERAPY. 27 (2018) 293–302. https://doi.org/10.5978/islsm.27_18-RA-01.
[5] V. Sol, P. Branland, V. Chaleix, R. Granet, M. Guilloton, F. Lamarche, B. Verneuil, P. Krausz, Amino porphyrins as photoinhibitors of Gram-positive and -negative bacteria, Bioorganic & Medicinal Chemistry Letters. 14 (2004) 4207–4211. https://doi.org/10.1016/j.bmcl.2004.06.016.
[6] Y.N. Konan, R. Gurny, E. Allémann, State of the art in the delivery of photosensitizers for photodynamic therapy, Journal of Photochemistry and Photobiology B: Biology. 66 (2002) 89–106. https://doi.org/10.1016/S1011-1344(01)00267-6.
[7] M. Nisnevitch, F. Nakonechny, Y. Nitzan, Photodynamic antimicrobial chemotherapy by liposome-encapsulated water-soluble photosensitizers, Russ J Bioorg Chem. 36 (2010) 363–369. https://doi.org/10.1134/S106816201003012X.
[8] G. Fuhrmann, A. Serio, M. Mazo, R. Nair, M.M. Stevens, Active loading into extracellular vesicles significantly improves the cellular uptake and photodynamic effect of porphyrins, Journal of Controlled Release. 205 (2015) 35–44. https://doi.org/10.1016/j.jconrel.2014.11.029.
[9] A.P. Gerola, P.F.A. Costa, F.A.P. de Morais, T.M. Tsubone, A.O. Caleare, C.V. Nakamura, K. Brunaldi, W. Caetano, E. Kimura, N. Hioka, Liposome and polymeric micelle-based delivery systems for chlorophylls: Photodamage effects on Staphylococcus aureus, Colloids and Surfaces B: Biointerfaces. 177 (2019) 487–495. https://doi.org/10.1016/j.colsurfb.2019.02.032.
[10] O. Mertins, I.O.L. Bacellar, F. Thalmann, C.M. Marques, M.S. Baptista, R. Itri, Physical Damage on Giant Vesicles Membrane as a Result of Methylene Blue Photoirradiation, Biophysical Journal. 106 (2014) 162–171. https://doi.org/10.1016/j.bpj.2013.11.4457.
[11] I.O.L. Bacellar, M.C. Oliveira, L.S. Dantas, E.B. Costa, H.C. Junqueira, W.K. Martins, A.M. Durantini, G. Cosa, P. Di Mascio, M. Wainwright, R. Miotto, R.M. Cordeiro, S. Miyamoto, M.S. Baptista, Photosensitized Membrane Permeabilization Requires Contact-Dependent Reactions between Photosensitizer and Lipids, J. Am. Chem. Soc. 140 (2018) 9606–9615. https://doi.org/10.1021/jacs.8b05014.
[12] T. Lajunen, L.-S. Kontturi, L. Viitala, M. Manna, O. Cramariuc, T. Róg, A. Bunker, T. Laaksonen, T. Viitala, L. Murtomäki, A. Urtti, Indocyanine Green-Loaded Liposomes for Light-Triggered Drug Release, Mol. Pharmaceutics. 13 (2016) 2095–2107. https://doi.org/10.1021/acs.molpharmaceut.6b00207.
[13] Q. Li, W. Li, H. Di, L. Luo, C. Zhu, J. Yang, X. Yin, H. Yin, J. Gao, Y. Du, J. You, A photosensitive liposome with NIR light triggered doxorubicin release as a combined photodynamic-chemo therapy system, Journal of Controlled Release. 277 (2018) 114–125. https://doi.org/10.1016/j.jconrel.2018.02.001.
[14] J. Massiot, V. Rosilio, A. Makky, Photo-triggerable liposomal drug delivery systems: from simple porphyrin insertion in the lipid bilayer towards supramolecular assemblies of lipid–porphyrin conjugates, J. Mater. Chem. B. 7 (2019) 1805–1823. https://doi.org/10.1039/C9TB00015A.
[15] Y.-D. Sun, Y.-X. Zhu, X. Zhang, H.-R. Jia, Y. Xia, F.-G. Wu, Role of Cholesterol Conjugation in the Antibacterial Photodynamic Therapy of Branched Polyethylenimine-

Containing Nanoagents, Langmuir. 35 (2019) 14324–14331. https://doi.org/10.1021/acs.langmuir.9b02727.
[16] J. Godard, F. Brégier, P. Arnoux, B. Myrzakhmetov, Y. Champavier, C. Frochot, V. Sol, New Phenalenone Derivatives: Synthesis and Evaluation of Their Singlet Oxygen Quantum Yield, ACS Omega. 5 (2020) 28264–28272. https://doi.org/10.1021/acsomega.0c04172.
[17] A. Späth, C. Leibl, F. Cieplik, K. Lehner, J. Regensburger, K.-A. Hiller, W. Bäumler, G. Schmalz, T. Maisch, Improving Photodynamic Inactivation of Bacteria in Dentistry: Highly Effective and Fast Killing of Oral Key Pathogens with Novel Tooth-Colored Type-II Photosensitizers, J. Med. Chem. 57 (2014) 5157–5168. https://doi.org/10.1021/jm4019492.
[18] D. Muehler, K. Sommer, S. Wennige, K.-A. Hiller, F. Cieplik, T. Maisch, A. Späth, Light-activated phenalen-1-one bactericides: efficacy, toxicity and mechanism compared with benzalkonium chloride, Future Microbiology. 12 (2017) 1297–1310. https://doi.org/10.2217/fmb-2016-0229.
[19] F. Cieplik, F. Wimmer, D. Muehler, T. Thurnheer, G.N. Belibasakis, K.-A. Hiller, T. Maisch, W. Buchalla, Phenalen-1-One-Mediated Antimicrobial Photodynamic Therapy and Chlorhexidine Applied to a Novel Caries Biofilm Model, Caries Res. 52 (2018) 447–453. https://doi.org/10.1159/000487815.
[20] A. Posadaz, N.M. Correa, M.A. Biasutti, N.A. GarcÃ-a, A Kinetic Study of the Photodynamic Effect on Tryptophan Methyl Ester and Tryptophan Octyl Ester in DOPC Vesicles, Photochemistry and Photobiology. 86 (2010) 96–103. https://doi.org/10.1111/j.1751-1097.2009.00641.x.
[21] L. Gibot, A. Lemelle, U. Till, B. Moukarzel, A.-F. Mingotaud, V. Pimienta, P. Saint-Aguet, M.-P. Rols, M. Gaucher, F. Violleau, C. Chassenieux, P. Vicendo, Polymeric Micelles Encapsulating Photosensitizer: Structure/Photodynamic Therapy Efficiency Relation, Biomacromolecules. 15 (2014) 1443–1455. https://doi.org/10.1021/bm5000407.
[22] E. Temizel, T. Sagir, E. Ayan, S. Isik, R. Ozturk, Delivery of lipophilic porphyrin by liposome vehicles: Preparation and photodynamic therapy activity against cancer cell lines, Photodiagnosis and Photodynamic Therapy. 11 (2014) 537–545. https://doi.org/10.1016/j.pdpdt.2014.07.006.
[23] E. Nathan, K. Vijayashree, A. Harikrishna, M. Takafuji, H. Jintoku, H. Ihara, N.M. Rao, A novel photosensitizer: An L -glutamide lipid conjugate with improved properties for photodynamic therapy, Photochem. Photobiol. Sci. 15 (2016) 1476–1483. https://doi.org/10.1039/C6PP00304D.
[24] M. Merchán, T.S. Ouk, P. Kubát, K. Lang, C. Coelho, V. Verney, S. Commereuc, F. Leroux, V. Sol, C. Taviot-Guého, Photostability and photobactericidal properties of porphyrin-layered double hydroxide–polyurethane composite films, J. Mater. Chem. B. 1 (2013) 2139. https://doi.org/10.1039/c3tb20070a.
[25] F. Le Guern, V. Sol, C. Ouk, P. Arnoux, C. Frochot, T.-S. Ouk, Enhanced Photobactericidal and Targeting Properties of a Cationic Porphyrin following the Attachment of Polymyxin B, Bioconjugate Chem. 28 (2017) 2493–2506. https://doi.org/10.1021/acs.bioconjchem.7b00516.
[26] F. Le Guern, T.-S. Ouk, C. Ouk, R. Vanderesse, Y. Champavier, E. Pinault, V. Sol, Lysine Analogue of Polymyxin B as a Significant Opportunity for Photodynamic Antimicrobial Chemotherapy, ACS Med. Chem. Lett. 9 (2018) 11–16. https://doi.org/10.1021/acsmedchemlett.7b00360.

[27] V. Rossa, G. Chenard Díaz, G. Juvenal Muchave, D. Alexandre Gomes Aranda, S. Berenice Castellã Pergher, Production of Solketal Using Acid Zeolites as Catalysts, in: M. Frediani, M. Bartoli, L. Rosi (Eds.), Glycerine Production and Transformation - An Innovative Platform for Sustainable Biorefinery and Energy, IntechOpen, 2019. https://doi.org/10.5772/intechopen.85817.
[28] H.E. Ries, H.D. Cook, Monomolecular films of mixtures, Journal of Colloid Science. 9 (1954) 535–546. https://doi.org/10.1016/0095-8522(54)90056-2.
[29] K. Hąc-Wydro, P. Wydro, The influence of fatty acids on model cholesterol/phospholipid membranes, Chemistry and Physics of Lipids. 150 (2007) 66–81. https://doi.org/10.1016/j.chemphyslip.2007.06.213.
[30] L.H.R.R. Possarle, J.R. Siqueira Junior, L. Caseli, Insertion of carbon nanotubes in Langmuir-Blodgett films of stearic acid and asparaginase enhancing the catalytic performance, Colloids and Surfaces B: Biointerfaces. 192 (2020) 111032. https://doi.org/10.1016/j.colsurfb.2020.111032.
[31] C.M. Hollinshead, R.D. Harvey, D.J. Barlow, J.R.P. Webster, A.V. Hughes, A. Weston, M.J. Lawrence, Effects of Surface Pressure on the Structure of Distearoylphosphatidylcholine Monolayers Formed at the Air/Water Interface †, Langmuir. 25 (2009) 4070–4077. https://doi.org/10.1021/la8028319.
[32] P. Wydro, S. Knapczyk, M. Łapczyńska, Variations in the Condensing Effect of Cholesterol on Saturated versus Unsaturated Phosphatidylcholines at Low and High Sterol Concentration, Langmuir. 27 (2011) 5433–5444. https://doi.org/10.1021/la105142w.
[33] A. Botet-Carreras, M.T. Montero, Ò. Domènech, J.H. Borrell, Effect of cholesterol on monolayer structure of different acyl chained phospholipids, Colloids and Surfaces B: Biointerfaces. 174 (2019) 374–383. https://doi.org/10.1016/j.colsurfb.2018.11.040.
[34] P. Dynarowicz-Łatka, V. Rosilio, P. Boullanger, P. Fontaine, M. Goldmann, A. Baszkin, Influence of a Neoglycolipid and Its PEO–Lipid Moiety on the Organization of Phospholipid Monolayers, Langmuir. 21 (2005) 11941–11948. https://doi.org/10.1021/la051749w.
[35] T. Komatsu, M. Moritake, E. Tsuchida, Molecular Energy and Electron Transfer Assemblies Made of Self-Organized Lipid-Porphyrin Bilayer Vesicles, Chem. Eur. J. 9 (2003) 4626–4633. https://doi.org/10.1002/chem.200305013.
[36] J.F. Lovell, C.S. Jin, E. Huynh, H. Jin, C. Kim, J.L. Rubinstein, W.C.W. Chan, W. Cao, L.V. Wang, G. Zheng, Porphysome nanovesicles generated by porphyrin bilayers for use as multimodal biophotonic contrast agents, Nature Mater. 10 (2011) 324–332. https://doi.org/10.1038/nmat2986.
[37] J. Massiot, V. Rosilio, N. Ibrahim, A. Yamamoto, V. Nicolas, O. Konovalov, M. Tanaka, A. Makky, Newly Synthesized Lipid–Porphyrin Conjugates: Evaluation of Their Self-Assembling Properties, Their Miscibility with Phospholipids and Their Photodynamic Activity In Vitro, Chem. Eur. J. 24 (2018) 19179–19194. https://doi.org/10.1002/chem.201804865.
[38] L.J. Lis, M. McAlister, N. Fuller, R.P. Rand, V.A. Parsegian, Interactions between neutral phospholipid bilayer membranes., Biophys J. 37 (1982) 657–665.
[39] J. Pan, S. Tristram-Nagle, J.F. Nagle, Effect of cholesterol on structural and mechanical properties of membranes depends on lipid chain saturation, Phys. Rev. E. 80 (2009) 021931. https://doi.org/10.1103/PhysRevE.80.021931.

[40] P. Smith, D.M. Owen, C.D. Lorenz, M. Makarova, Asymmetric phospholipids impart novel biophysical properties to lipid bilayers allowing environmental adaptation, Biophysics, 2020. https://doi.org/10.1101/2020.06.03.130450.
[41] X. Wu, B. Chantemargue, F. Di Meo, C. Bourgaux, D. Chapron, P. Trouillas, V. Rosilio, Deciphering the Peculiar Behavior of β-Lapachone in Lipid Monolayers and Bilayers, Langmuir. 35 (2019) 14603–14615. https://doi.org/10.1021/acs.langmuir.9b02886.
[42] M. N'Diaye, J. Vergnaud-Gauduchon, V. Nicolas, V. Faure, S. Denis, S. Abreu, P. Chaminade, V. Rosilio, Hybrid Lipid Polymer Nanoparticles for Combined Chemo- and Photodynamic Therapy, Mol. Pharmaceutics. 16 (2019) 4045–4058. https://doi.org/10.1021/acs.molpharmaceut.9b00797.
[43] B.B. Gerbelli, E.R. da Silva, B. Miranda Soares, W.A. Alves, E. Andreoli de Oliveira, Multilamellar-to-Unilamellar Transition Induced by Diphenylalanine in Lipid Vesicles, Langmuir. 34 (2018) 2171–2179. https://doi.org/10.1021/acs.langmuir.7b03869.
[44] S. Shi, T. Yin, W. Shen, Multilamellar to unilamellar vesicle transformation in aqueous solutions of a catanionic surface active ionic liquid, Journal of Molecular Liquids. 290 (2019) 111245. https://doi.org/10.1016/j.molliq.2019.111245.

Graphical abstract